EurJOC European Journal of Organic Chemistry

FULL PAPER

DOI: 10.1002/ejoc.201500549

# Chiral Gold Nanoparticles Decorated with Pseudopeptides

**Rossana Fanelli,[a] Lorenzo Milli,[b] Andrea Cornia,[c] Alessandro Moretto,[d] Nicola Castellucci,[b] Nicola Zanna,[b] Giulia Malachin,[d] Regina Tavano,[e] and Claudia Tomasini*[b]**

**Keywords:** Nanoparticles / Gold / Peptidomimetics / Foldamers / Circular dichroism / Conformation analysis

Peptide-functionalized gold nanoparticles are supramolecular systems that can mimic natural proteins or DNA. In this work, we describe the preparation, the analysis, and the biological evaluation of gold nanoparticles linked to pseudopeptide foldamers containing one to eight L-Ala-D-Oxd (Ala = alanine; Oxd = 4-carboxy-5-methyloxazolidin-2-one) residues. The nanoparticles become increasingly organized as the number of such moieties increases. Moreover, from the analysis of chiroptical signals we find that the chirality of the gold surface becomes more evident with decreasing foldamer length. Finally, these systems display no cytotoxicity towards HeLa cells and are good candidates to promote drug delivery once equipped with biologically active moieties.

## Introduction

Colloidal solutions have been known and widely used since antiquity.[1] However, colloid science had development at a slower pace compared with other branches of chemistry because of several difficulties encountered in the preparation, reproduction, and characterization of colloidal solutions.

More recently, nanoparticles (NPs) functionalized with various molecular and biomolecular units were assembled into complex hybrid systems.[2] Composite layered or aggregated structures of (macro)molecule-cross-linked NPs on surfaces have been prepared,[3] and specific sensing of substrates, tunable electroluminescence, and enhanced photoelectrochemistry[4] have been observed. Several reviews have addressed the recent advances in the synthesis and properties of NPs[5] and the progress made in the integration of composite NP systems with surfaces.[6]

Peptide-functionalized gold nanoparticles (AuNPs)[7] are intriguing supramolecular systems that can mimic natural proteins or DNA. A cluster of gold atoms surrounded by copies of a peptide is a nanosystem that resembles a protein in size (2–20 nm), shape (globular), and, possibly, function.

A variety of synthetic methodologies for the preparation of AuNPs within a narrow size distribution are available.[8] Such systems may be assembled by "wet chemistry" procedures, whereby a surface-capping ligand binds to the metal, controlling its growth and avoiding agglomeration or coalescence into the bulk material.[9]

The design strategy for the synthesis of a peptide-based capping ligand must address some key requirements. For instance, it is important to avoid attractive interparticle interactions promoted by ammonium and carboxylate groups. Moreover, peptides need to have a strong affinity for gold and must be able to self-assemble into a dense layer that excludes water, while a hydrophilic terminus is required to achieve solubility and stability in water.[10]

In this work, we describe the preparation, the analysis, and the biological evaluation of AuNPs capped by pseudopeptide foldamers containing the L-Ala-D-Oxd (Ala = alanine; Oxd = 4-carboxy-5-methyloxazolidin-2-one) moiety and functionalized with a trityl mercaptopropanoic linker (Figure 1). In our previous work we fully demonstrated that oligomers containing several L-Ala-D-Oxd residues tend to become organized into β-bend ribbon spirals.[11]

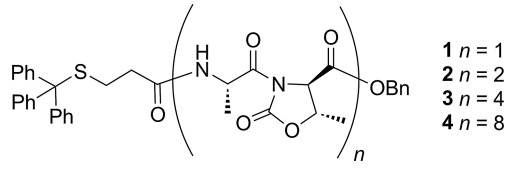


Figure 1. General structure of the pseudopeptide foldamers described in this work.

[a] School of Chemistry Food & Pharmacy, University of Reading, Whiteknights, P. O. Box 217, Reading, Berkshire, RG6 6AH, United Kingdom
[b] Departimento di Chimica "G. Ciamician", Università di Bologna,
2, Via Selmi, 40126 Bologna, Italy
E-mail: claudia.tomasini@unibo.it
[c] Dipartimento di Scienze Chimiche e Geologiche, University of Modena and Reggio Emilia,
183, Via G. Campi, 41125 Modena, Italy
[d] Dipartimento di Scienze Chimiche, Università di Padova,
1, Via Marzolo, 35131 Padova, Italy
[e] Dipartimento di Scienze Biomediche, Università di Padova,
3, Viale G. Colombo, 35121 Padova, Italy
Supporting information for this article is available on the WWW under http://dx.doi.org/10.1002/ejoc.201500549.

  

## Results and Discussion

### Synthesis

We prepared a series of oligomers Boc-(L-Ala-D-Oxd)$_n$-OBn ($n$ = 1, 2, 4, 8) (Boc = *tert*-butyloxycarbonyl) (Scheme 1) by conventional methods in solution, starting from L-Ala and D-Thr (Thr = threonine). Boc-L-Ala-D-Oxd-OBn (**5**) was obtained in high yield by addition of Boc-L-Ala-OH to D-Oxd-OBn in the presence of *O*-(benzotriazol-1-yl)-*N*,*N*,*N*′,*N*′-tetramethyluronium hexafluorophosphate (HBTU) and triethylamine (TEA) in anhydrous acetonitrile,[12] whereas D-Oxd-OBn can be easily synthesized in multigram scale starting from D-Thr.

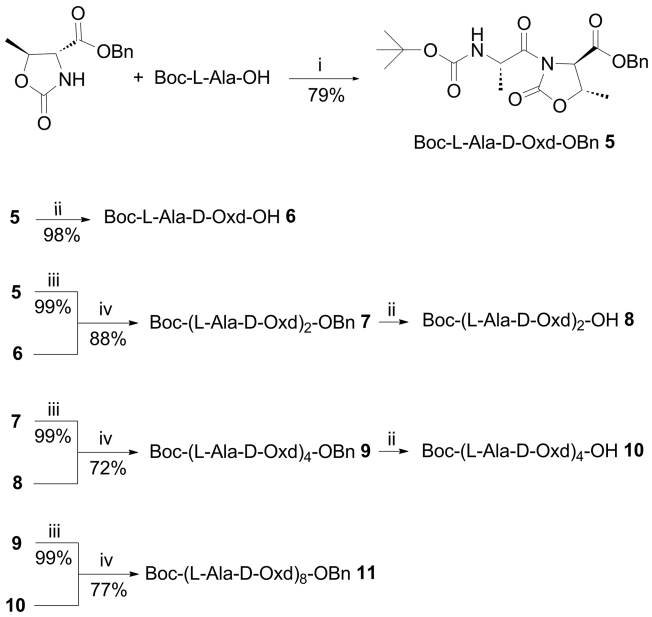


Scheme 1. Reagents and conditions: (i) HBTU (1.1 equiv.), TEA (2 equiv.), anhydrous $CH_3CN$, 1 h, r.t.; (ii) $H_2$, Pd/C (10%), MeOH, 16 h, r.t.; (iii) TFA (18 equiv.), anhydrous $CH_2Cl_2$, 4 h, r.t.; (iv) HBTU (1.1 equiv.), TEA (3 equiv.), anhydrous $CH_3CN$, 1 h, r.t.

The other oligomers **7**, **9**, and **11** were synthesized in solution by selective deprotection of the C-terminal benzyl esters with $H_2$ in methanol in the presence of Pd/C (10%) and by cleavage of the N-terminal Boc moieties with anhydrous trifluoroacetic acid (TFA) in dichloromethane. The two deprotected moieties were then coupled by using HBTU and TEA in anhydrous acetonitrile under an inert atmosphere to give the longer oligomers in satisfactory yield. All the deprotection steps were performed with excellent yields, whereas the yields of the coupling step ranged from 72 to 88% (Scheme 1).

Compounds **1**–**4** were prepared by cleavage of the N-terminal Boc moieties with anhydrous TFA in dichloromethane followed by coupling with trityl mercaptopropionic acid in the presence of HBTU and TEA in acetonitrile at room temperature under a nitrogen atmosphere (Scheme 2). The reaction was complete after one hour and the desired compounds were obtained with a yield ranging from 52 to 63%.

### Conformational Analysis of 1–4

Before linking compounds **1**–**4** to AuNPs, the possible adoption of a well-defined secondary structure in these compounds, as in the previously studied *N*-Boc derivatives,[13] was investigated by IR and NMR spectroscopy and by single-crystal X-ray diffraction. The N–H stretching region enables intramolecular C=O···H–N hydrogen bonds formed in solution to be detected; free (non-hydrogen-bonded) amide NH groups exhibit a stretching signal above 3400 cm$^{-1}$, whereas hydrogen-bonded amides[14] produce a stretching band below 3400 cm$^{-1}$. The FTIR spectra were recorded in $CH_2Cl_2$ at a compound concentration of 3 mM, so as to avoid compound self-aggregation (Table S1, for the IR spectra see the Supporting Information).

The spectrum of **1** clearly shows the presence of only one band at 3419 cm$^{-1}$ attributed to free amide groups. By contrast, two bands at 3436 and 3347 cm$^{-1}$ are seen in the spectrum of **2**, indicating that both free and hydrogen-bonded amide NH groups are present in solution. Significantly, the stretching band above 3400 cm$^{-1}$ disappears in **3** and **4**, suggesting that these compounds adopt a folded conformation, as could be anticipated from the analysis of their N-Boc protected counterparts.[13] A similar trend was observed for the C=O stretching band of the amide groups, which shift from 1679 cm$^{-1}$ in **1** to 1663 cm$^{-1}$ in **4**.

$^1$H NMR analysis supports the foregoing interpretation of IR spectroscopy results. The NH group of **1** resonates at $\delta$ = 6.08 ppm, whereas the NH groups of **2** resonate at $\delta$ = 5.94 and 7.35 ppm and the NH groups of **4** are very deshielded, ranging between 7.9 and 8.5 ppm; these pronounced downfield shifts are usually indicative of hydrogen-bonded NH groups.[14] The occurrence of intramolecular C=O···H–N hydrogen bonds in oligomers **2** and **4** was further confirmed by following the dependence of NH proton chemical shifts upon addition of [$D_6$]dimethyl sulfoxide ([$D_6$]DMSO). This solvent is a strong hydrogen-bond acceptor and, when bound to a NH proton, it is expected to have a dramatic deshielding effect.[15] The results of [$D_6$]-

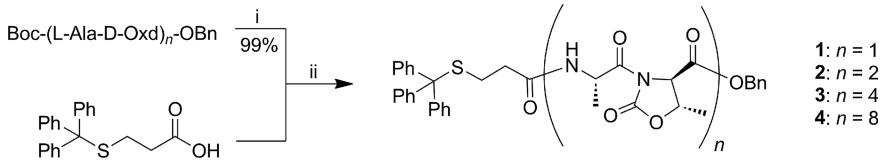


Scheme 2. Reagents and conditions: (i) TFA (18 equiv.), anhydrous $CH_2Cl_2$, 4 h, r.t.; (ii) HBTU (1.1 equiv.), TEA (2 equiv.), anhydrous $CH_3CN$, 1 h, r.t.

  

DMSO/$CDCl_3$ titrations of the NH protons in pseudopeptides **2** and **4** are presented in Figure 2.

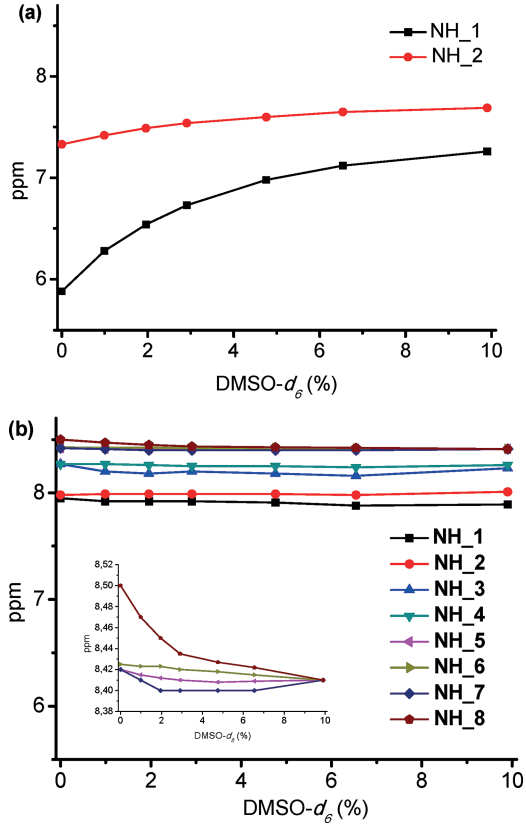


Figure 2. Variation of NH proton chemical shifts (ppm) of **2** (a), and **4** (b) as a function of increasing percentages of [$D_6$]DMSO added to the $CDCl_3$ solution (v/v) (concentration: 3 mM).

Of the two NH protons in **2**, one is totally free ($\Delta\delta$ = 1.40 ppm over the explored range of DMSO concentration), whereas the second is quite H-bonded ($\Delta\delta$ = 0.34 ppm). The former is most likely the group closer to the S terminus, because its chemical shift in $CDCl_3$ solution is virtually the same as that found in compound **1**. By contrast, all NH protons in **4** are DMSO-insensitive, confirming that **4** is fully organized in a secondary structure supported by C=O···H–N interactions.

X-ray quality crystals of **2** were grown as long colorless needles by slow evaporation of a toluene solution. Unfortunately we were not able to grow crystals of oligomers **1**, **3**, or **4**. Crystal data and refinement parameters for **2** are given in Table S2; the geometry of hydrogen-bond interactions are detailed in Table S3 and conformational data are gathered in Table S4. The crystals are monoclinic, space group $P2_1$, and the unit cell comprises two molecules related by the twofold screw axis (Figure 3). The molecule exhibits a turn-like structure. As found in related foldamers,[16] the L-Ala1 α-carbon atom C22 has a H-contact with the endocyclic C=O of the neighboring D-Oxd1 residue [$d$(H22···O8) = 2.300(13) Å]. However, no significant H-bonding interaction is established between the carbonyl oxygen O10 and the amide group N2–HN2 of L-Ala2 [$d$(HN2···O10) = 2.808(16) Å], so that a ten-membered hydrogen-bonded turn ($3_{10}$-helical structure) is not formed. Instead, the strongest intramolecular H-bonding interaction involves amide nitrogen N2 and the D-Oxd2 carbonyl oxygen O4 [$d$(HN2···O4) = 2.141(18) Å]. Notably, the amide group N4–HN4 of L-Ala1 is not engaged in intramolecular hydrogen bonds in the solid state, and the resulting picture matches remarkably well the results of IR and $^1$H NMR investigations in solution. Molecules related by the $2_1$ axis are hydrogen bonded into chains through amide group N4–HN4 and carbonyl oxygen O4 [$d$(HN4···O4$^i$) = 2.103(11) Å], but crystal packing also relies on a number of other short C–H···O contacts (Table S3). The backbone conformational parameters gathered in Table S4 show that the torsion angles (ϕ and ψ) at the L-Ala1 residue are similar to those of poly-L-proline II helix, as in related foldamers.[16] However, the L-Ala2 residue has quite different conformational parameters that fall in the right-handed α-helix region of the Ramachandran plot.

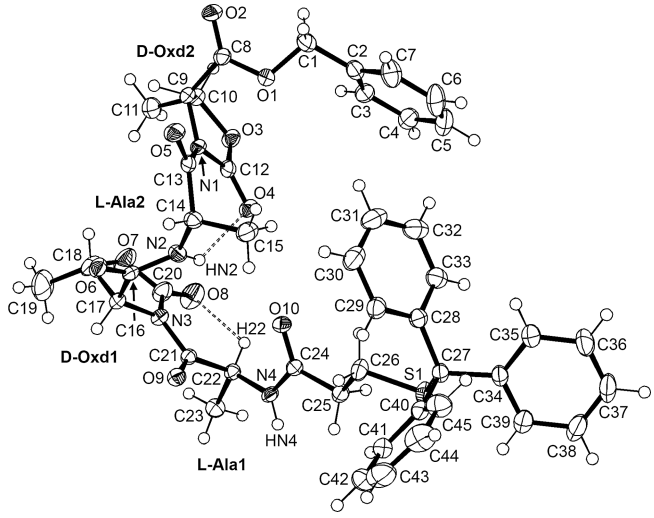


Figure 3. Partially labeled ORTEP-3[18] plot of **2** with displacement ellipsoids at 50% probability level and H atoms drawn as spheres with arbitrary radius. Dashed lines indicate intramolecular hydrogen-bonding interactions discussed in the text. For simplicity, only H atoms engaged in intra- or intermolecular hydrogen bonds have been labeled. Atom labeling follows the system used previously.[16]

The ECD spectra of compounds **1**–**4** were not recorded because the spectral features related to the secondary structure are obscured around 200 nm by the very strong B transitions of trityl groups, that are removed upon formation of the AuNPs. Strong support for the formation of a robust secondary structure for the longer oligomers of the (L-Ala-D-Oxd)$_n$ series comes from analysis of the Boc-(L-Ala-D-Oxd)$_n$-OH oligomers, that we reported previously.[11] We could demonstrate that a stable $3_{10}$ helix is formed when $n \geq 5$.

## Preparation and Analysis of Gold Nanoparticles

Pseudopeptide-functionalized gold nanoparticles AuNPs**1**, AuNPs**2**, AuNPs**3**, AuNPs**4** were obtained by reduction of

  

$HAuCl_4$ with $NaBH_4$ in the presence of compounds **1**–**4**, respectively.

Structural information on the NPs was obtained by using several techniques (Table 1). The average number of Au atoms per NP was calculated by assuming spherical particles and using the diameter of the metallic core observed in transmission electron microscopy (TEM) images and the density of bulk metal (55 atoms/nm$^3$) (Figure S3).

Table 1. Chemical structure data for AuNPs**1**–**4**.

| AuNP | Core diameter [nm][a] | No. of Au atoms per NP[b] | No. of foldamers per NP[c] | Footprint [nm$^2$][d] |
|---|---|---|---|---|
| AuNPs**1** | 2.1 ± 0.3 | 289 | 167 | 0.10 |
| AuNPs**2** | 2.3 ± 0.3 | 376 | 156 | 0.11 |
| AuNPs**3** | 2.3 ± 0.4 | 376 | 135 | 0.15 |
| AuNPs**4** | 2.5 ± 0.3 | 508 | 97 | 0.56 |

[a] Calculated by averaging the size of at least 200 NPs. [b] Calculated by assuming a spherical model. [c] Determined by combining TEM and TGA analysis, as described in the Supporting Information. [d] Defined as the area occupied by the projection of the foldamer ligand onto the gold cluster surface.

The number of foldamers conjugated to the inorganic core was calculated by using the weight loss observed in thermogravimetric analysis (TGA),[17] assumed to arise from the loss of the organic coating monolayer, and the molecular weight of the appropriate oligomer (Figure S4).

Finally the foldamer footprints were calculated by relating the number of oligomers linked to the gold surface with the dimensional information obtained by TEM analysis (Figure S5).

The UV/Vis absorption spectra (Figure 4) are consistent with the results gathered in Table 1, because a plasmonic band (ca. 520 nm) indicative of a NP diameter ≥ 2.5 nm was observed only for AuNPs**4**.[19]

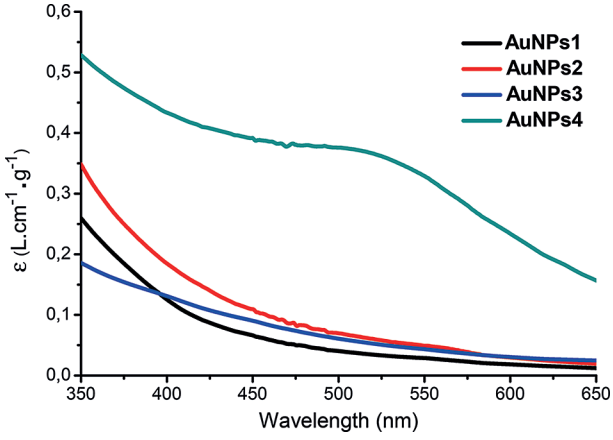


Figure 4. UV/Vis spectra of AuNPs**1**–**4** recorded in $H_2O$ at 20 °C in the 350–650 nm region.

Another important feature of AuNPs is chirality, which may derive from several factors:[20] (1) A chiral arrangement of metal atoms in the core; (2) the binding of thiolates on the gold surface to form chirally arranged staples; (3) the chirality of the monolayer of passivating organic molecules. Pseudopeptide oligomers, binding to the gold core, may influence the whole NP to assume a diverse organization.

Electronic circular dichroism (ECD) analysis of AuNPs**1**–**4** was performed in water solution (Figure 5), both in the far-UV region (190–250 nm) and in the UV/Vis region (300–700 nm), where chiroptical signals are expected to arise from the chirality of the gold surface (chiral staples).

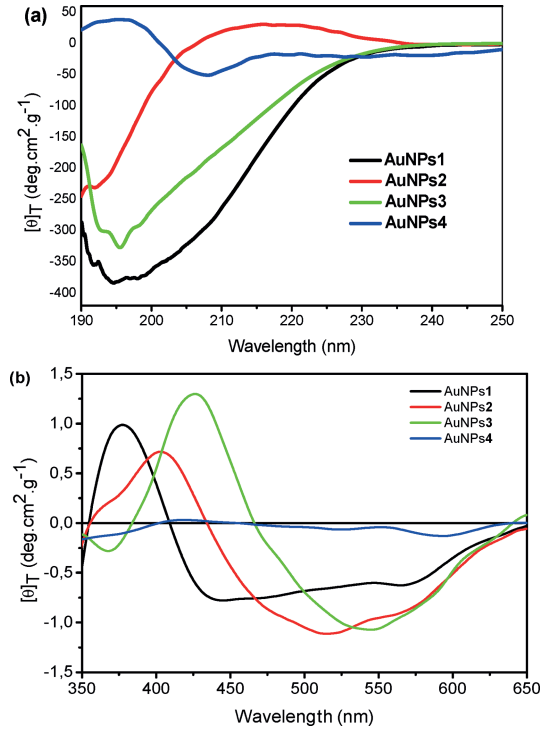


Figure 5. ECD spectra of AuNPs**1**–**4** recorded in water at 20 °C: (a) far-UV ECD spectra indicating the foldamer chirality; (b) UV/Vis ECD spectra indicating the chirality of the gold surface.

The ECD spectra in the far-UV region are reported for AuNPs**1**–**4** in Figure 5 (a). The spectra of AuNPs**1** and AuNPs**3** show only a deep minimum at 195 nm, which is usually associated with a random coil conformation,[21] whereas AuNPs**2** shows a deep minimum at 191 nm and a weak maximum at 215 nm. All these spectra resemble closely those of unordered peptides,[21] the ECD response of which entails a strong negative band near 197 nm and a weak band at approximately 220 nm, that may be a negative shoulder on the short-wavelength band. In contrast, the spectrum of AuNPs**4** outlines the typical conformation of a $3_{10}$ helix, displaying a maximum at 195 nm, a deep minimum at 208 nm, and a shoulder at 227 nm.[22] The four separate ECD spectra of AuNPs**1**–**4** are reported in Figure S6.

The chiroptical signals associated with the gold surface are reported in Figure 5 (b).[23] The signals associated with AuNPs**1**–**3** show a variation of the molar ellipticity, with a maximum ranging between 360 and 430 nm, whereas AuNPs**4** shows a steadier trend. This outcome suggests that only an unordered conformation may influence the chirality of the whole AuNP, whereas the more robust secondary structure **4** does not communicate with the AuNPs. This is a remarkable effect that confirms previous observations on AuNPs passivated with short oligopeptides based on Aib-L-Ala repeating units (Aib = aminoisobutyric acid).[24] These NPs presented

  

relevant ECD signals in the 300–650 nm wavelength region only for short peptides. These signals vanished when the sequences were long enough to assume a folded conformation.

### Effect of AuNPs on Cell Viability

The cytotoxic acute effect of the different AuNPs developed in this study was evaluated in HeLa cells, which is a human cell line from cervical cancer. After incubation at different nanoparticle concentrations, cell viability was assessed by the MTS assay. In this test, the MTS compound is reduced by living cells into a colored formazan product that is soluble in tissue culture medium. So, the quantity of formazan, the absorbance of which was measured at 490 nm, is directly proportional to the number of living cells in the culture. As shown in Figure 6, none of the four types of AuNPs used are toxic for human HeLa cells up the high dose of 200 μg/mL.

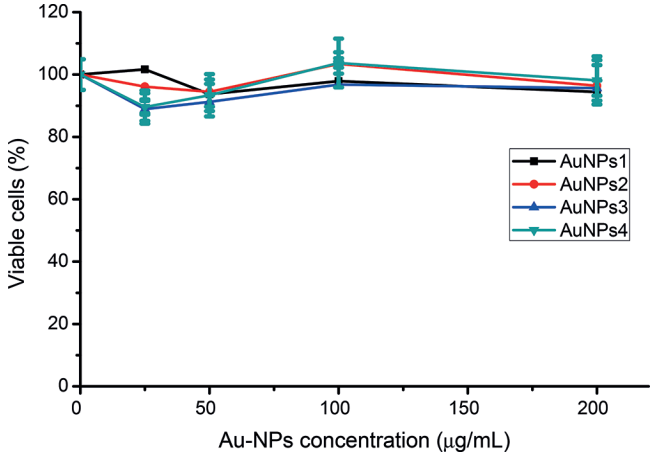


Figure 6. Cell viability evaluated in HeLa cells by the MTS assay, after incubation for 24 h with different concentrations of NPs. The percentage of living cells was calculated with respect to control cells (no NPs). Values are mean ± SE ($N$ = 2).

We also determined the ability of AuNPs to induce the production of reacting oxygen species (ROS). To this end, HeLa cells were incubated with AuNPs**1**–**4** for three hours and the produced ROS were measured using the Carboxy-H2DCFDA (6-carboxy-2′,7′-dichlorodihydrofluorescein diacetate) probe. This nonfluorescent molecule is converted into a green-fluorescent form by ROS, as they remove the acetate groups.

As shown in Figure S7, in spite of their lack of cytotoxicity, all AuNPs can induce ROS production. AuNPs**1** was the least active, whereas AuNPs**3** induced the strongest ROS production.

## Conclusions

Gold nanoparticles capped with pseudopeptide foldamers based on the L-Ala-D-Oxd repeating unit and featuring a terminal mercaptopropanoic linker were prepared and analyzed. With increasing number of L-Ala-D-Oxd units ($n$ = 1, 2, 4, and 8), the pseudopeptides become increasingly more organized in their secondary structure, as shown by the combined use of IR and NMR spectroscopy and X-ray crystallography. In particular, both in solution and in the solid state, only one NH group of the (L-Ala-D-Oxd)$_2$ moiety is engaged in intramolecular H-bonding interactions. By contrast, all NH groups of the longer-chain derivatives are involved in intramolecular hydrogen bonds.

According to the ECD spectra, such a scenario is largely retained when pseudopeptide foldamers are linked to AuNPs, with the (L-Ala-D-Oxd)$_8$ moiety forming a well-organized $3_{10}$ helix.

Moreover, chiroptical signals in the UV/Vis region suggest that the chirality of the gold surface becomes more pronounced with decreasing foldamer length. This important outcome demonstrates that oligopeptide chirality may be communicated to the whole NPs with better efficiency through an unordered oligopeptide conformation than through a well-organized secondary structure.

Finally, regardless of their conformation, none of the capped AuNPs displayed acute cytotoxicity towards HeLa cells. However, detectable amounts of ROS were induced, with various efficacies, by all the studied AuNPs. Thus, these systems can be regarded as promising candidates for drug delivery once properly equipped with biologically active moieties.

## Experimental Section

**General:** Routine NMR spectra were recorded with spectrometers working at 400 or 200 MHz ($^1$H NMR) and at 100, 75 or 50 MHz ($^{13}$C NMR). Chemical shifts are reported in $\delta$ values relative to the solvent peak of $CHCl_3$ ($\delta$ = 7.27 ppm), $CH_3OH$ ($\delta$ = 3.31 ppm), and DMSO ($\delta$ = 2.54 ppm). Proton signals were assigned based on gCOSY spectra. IR spectra were recorded with an FTIR spectrometer. Melting points were determined in open capillaries and are uncorrected. High-quality infrared spectra (64 scans) were obtained at 2 cm$^{-1}$ resolution by using a 1 mm NaCl solution cell and a Bruker Laser class FT-infrared spectrometer. Spectra were recorded on 3 mM solutions in $CH_2Cl_2$ at 297 K. All compounds were dried in vacuo, and all sample preparations were performed in a nitrogen atmosphere. The ECD spectra were obtained with a Jasco J-810 spectropolarimeter. Cylindrical fused quartz cells of 0.02 cm and 1 cm path length were used. The values are expressed in terms of $[\theta]_T$, the total molar ellipticity (deg cm$^2$ g$^{-1}$). UV/Vis absorption spectra were measured in water with a Perkin–Elmer Lambda 45 UV/Vis spectrophotometer with 1 cm path length quartz cuvettes. TEM micrographs were registered with a Jeol 300PX instrument. Samples were prepared by 100-fold dilution of a 2 mg/mL Milli-Q water solution of the appropriate AuNPs**1**–**4**. A glow discharged carbon coated grid was floated on a small drop of solution and excess was removed by #50 hardened Whatman filter paper. TGA was run on 5–8 mg nanoparticle samples with a SDT-2960 model TA instrument from 25 to 1200 °C under a continuous $N_2$ flow.

Detailed information for the synthesis and characterization of oligomers are reported in the Supporting Information.

**Synthesis of AuNPs4:** Compound **4** (53 mg, 0.026 mmol) was dissolved in a mixture of Milli-Q water, MeOH, and $CH_2Cl_2$. A solution of $HAuCl_4$ (0.040 g, 0.11 mmol) in water was added and the mixture was stirred for 20 min to permit the polymerization. A solution of $NaBH_4$ (0.020 g, 0.53 mmol) dissolved in water was then added to the mixture very rapidly. A brown solution was obtained and, after 2 h, the reaction reached completion. The reaction was quenched by ad-

  

dition of 0.1 M HCl (1 mL). The solvent was removed under reduced pressure and the dark residue was dissolved in Milli-Q water (4 mL). Subsequently, the so-obtained solution was filtered through a 45 μm microfilter, the nanoparticles precipitated by adding a large amount of $CH_3CN$ and AuNPs**4** was finally isolated by centrifugation or filtration. This method was also applied for the preparation of AuNPs**1**–**3** samples.

**X-ray Crystallography:** Single-crystal X-ray structure determination on **2** was carried out at 140(2) K with a Bruker-Nonius X8APEX diffractometer equipped with Mo-$K_\alpha$ generator, area detector, and Kryoflex liquid nitrogen cryostat. The structure was solved in space group $P2_1$ and successfully refined on $F_o^2$ by standard methods, using SIR92[25] and SHELXL-97[26] software included in the WINGX v2013.3 suite.[27] All non-hydrogen atoms were refined anisotropically, whereas hydrogen atoms were treated with isotropic displacement (ID) parameters. Aromatic and methyl hydrogen atoms were added in idealized positions and allowed to ride on the parent carbon atom, with $U(H) = 1.2U_{eq}(C)$ and $U(H) = 1.5U_{eq}(C)$, respectively (torsion angle was refined for methyl groups using AFIX 137 instruction). The remaining hydrogen atoms were refined by forcing ID parameters to be identical within each methylene group, by restraining C–H distances to be the same (within 0.015 Å) for all tertiary and all methylene hydrogen atoms, and by fixing N–H distances to 0.880(15) Å. The expected absolute configuration at C9, C10, C14, C17, C18, and C22 was confirmed by anomalous dispersion effects; Flack parameter: 0.01(4).

CCDC-1060459 contains the supplementary crystallographic data for this paper. These data can be obtained free of charge from The Cambridge Crystallographic Data Centre via www.ccdc.cam.ac.uk/data_request/cif.

**Cell Culture and MTS Assay:** HeLa cells were maintained in DMEM medium (Gibco), supplemented with 10% FCS (Euroclone) and antibiotics (penicillin and streptomycin, Invitrogen) at 37 °C in a humidified atmosphere containing 5% (v/v) $CO_2$; cells were split every 2–3 d. The day before the experiment, cells were detached by trypsin treatment (Gibco), counted, and seeded onto 96 wells/plate ($50 \times 10^3$ cells/well, Falcon). Different nanoparticles were diluted in culture medium (up to 200 μg/mL) in DMEM supplemented with FCS and added to the cells. As a positive control, cells were treated with medium without stimuli. After 24 h treatment, cells were tested using a CellTiter 96 AQueous One Solution Reagent (Promega). Plates were read with an ELISA reader (Amersham Biosciences) at 490 nm. The percentage of viable cells was calculated with respect to data for the control cells.

## Acknowledgments

L. M., N. Z., R. T., G. M., and C. T. thank the Italian Ministero dell'Istruzione, dell'Università e della Ricerca (MIUR) (program PRIN 2010NRREPL_009) and the Consorzio Spinner Regione Emilia Romagna for financial support.

[1] Everett, D. H. *Principles of Colloid Science*, Royal Society of Chemistry, Paperbacks, **1988**.
[2] S. Knoppe, T. Bürgi, *Acc. Chem. Res.* **2014**, *47*, 1318–1326.
[3] a) M. Lahav, A. N. Shipway, I. Willner, *J. Chem. Soc. Perkin Trans. 2* **1999**, 1925–1931; b) W. Chen, D. Grouquist, J. Roark, *J. Nanosci. Nanotechnol.* **2002**, *2*, 47–53.
[4] A. N. Shipway, I. Willner, *Chem. Commun.* **2001**, 2035–2045.
[5] a) A. N. Shipway, E. Katz, I. Willner, *ChemPhysChem* **2000**, *1*, 18–52; b) T. Trindade, P. O' Brien, N. L. Pickett, *Chem. Mater.* **2001**, *13*, 3843–3858; c) J.-T. Lue, *J. Phys. Chem. Solids* **2001**, *62*, 1599–1612; d) K. Grieve, P. Mulvaney, F. Grieser, *Curr. Opin. Colloid Interface Sci.* **2000**, *5*, 168–172; e) P. Schwerdtfeger, *Angew. Chem. Int. Ed.* **2003**, *42*, 1892–1895; *Angew. Chem.* **2003**, *115*, 1936–1939.
[6] a) M. Brust, C. J. Kiely, *Colloids Surf. A* **2002**, *202*, 175–186; b) W. P. McConnell, J. P. Novak, L. C. Brousseau III, R. R. Fuierer, R. C. Tenent, D. L. Feldheim, *J. Phys. Chem. B* **2000**, *104*, 8925–8930; c) R. Gangopadhyay, A. De, *Chem. Mater.* **2000**, *12*, 608–622.
[7] M. C. Daniel, D. Astruc, *Chem. Rev.* **2004**, *104*, 293–346.
[8] *Metal Nanoparticles: Synthesis Characterization, and Application* (Eds.: D. L. Feldheim, C. A. Foss Jr.), Marcel Dekker, New York, **2002**.
[9] E. Katz, I. Willner, *Angew. Chem. Int. Ed.* **2004**, *43*, 6042–6108; *Angew. Chem.* **2004**, *116*, 6166.
[10] R. Lévy, N. T. K. Thanh, R. C. Doty, I. Hussain, R. J. Nichols, D. J. Schiffrin, M. Burst, D. G. Fernig, *J. Am. Chem. Soc.* **2004**, *126*, 10076–10084.
[11] C. Tomasini, G. Angelici, N. Castellucci, *Eur. J. Org. Chem.* **2011**, 3648–3669.
[12] a) G. Longhi, S. Abbate, F. Lebon, N. Castellucci, P. Sabatino, C. Tomasini, *J. Org. Chem.* **2012**, *77*, 6033–6042; b) G. Angelici, G. Luppi, B. Kaptein, Q. B. Broxterman, H.-J. Hofmann, C. Tomasini, *Eur. J. Org. Chem.* **2007**, 2713–2721.
[13] C. Tomasini, G. Luppi, M. Monari, *J. Am. Chem. Soc.* **2006**, *128*, 2410–2420.
[14] a) L. Belvisi, C. Gennari, A. Mielgo, D. Potenza, C. Scolastico, *Eur. J. Org. Chem.* **1999**, 389–400; b) J. Yang, S. H. Gellman, *J. Am. Chem. Soc.* **1998**, *120*, 9090–9091; c) I. G. Jones, W. Jones, M. North, *J. Org. Chem.* **1998**, *63*, 1505–1513; d) C. Toniolo, *CRC Crit. Rev. Biochem.* **1980**, *9*, 1–44; e) B. Imperiali, R. A. Moats, S. L. Fisher, T. J. Prins, *J. Am. Chem. Soc.* **1992**, *114*, 3182–3188.
[15] a) K. D. Kopple, M. Ohnishi, A. Go, *Biochemistry* **1969**, *8*, 4087–4095; b) D. Martin, H. G. Hauthal, in: *Dimethyl Sulphoxide*, Van Nostrand-Reinhold, Wokingham, UK, **1975**.
[16] L. Milli, M. Larocca, M. Tedesco, N. Castellucci, E. Ghibaudi, A. Cornia, M. Calvaresi, F. Zerbetto, C. Tomasini, *J. Org. Chem.* **2014**, *79*, 5958–5969.
[17] L. Fabris, S. Antonello, L. Armelao, R. L. Donkers, F. Polo, C. Toniolo, F. Maran, *J. Am. Chem. Soc.* **2006**, *128*, 326–336.
[18] L. J. Farrugia, *J. Appl. Crystallogr.* **1997**, *30*, 565–565.
[19] M. M. Alvarez, J. T. Khoury, T. G. Schaaff, M. N. Shafigullin, I. Vezmar, R. L. Whetten, *J. Phys. Chem. B* **1997**, *101*, 3706–3712.
[20] a) H. Alhassen, V. Antony, A. Ghanem, M. M. A. Yajadda, Z. J. Han, K. Ostrikov, *Chirality* **2014**, *26*, 683–691; b) H. Okamoto, T. Narushima, Y. Nishiyama, K. Imura, *Phys. Chem. Chem. Phys.* **2015**, *17*, 6192–6206.
[21] a) C. Toniolo, F. Formaggio, R. W. Woody, *Comprehensive Chiroptical Spectroscopy 2*, John Wiley & Sons, **2012**, 499–544; b) N. J. Greenfield, G. D. Fasman, *Biochemistry* **1969**, *8*, 4108–4116; c) M. L. Tiffany, S. Krimm, *Biopolymers* **1969**, *8*, 347–359; d) W. C. Johnson Jr., I. Tinoco Jr., *J. Am. Chem. Soc.* **1972**, *94*, 4389–4390.
[22] C. Toniolo, A. Polese, F. Formaggio, M. Crisma, J. Kamphuis, *J. Am. Chem. Soc.* **1996**, *118*, 2744–2745.
[23] I. M. Rio-Echevarria, R. Tavano, V. Causin, E. Papini, F. Mancin, A. Moretto, *J. Am. Chem. Soc.* **2011**, *133*, 8–11.
[24] E. Longo, A. Orlandin, F. Mancin, P. Scrimin, A. Moretto, *ACS Nano* **2013**, *7*, 9933–9939.
[25] A. Altomare, G. Cascarano, C. Giacovazzo, A. Guagliardi, *J. Appl. Crystallogr.* **1993**, *26*, 343–350.
[26] G. M. Sheldrick, *Acta Crystallogr., Sect. A* **2008**, *64*, 112–122.
[27] L. J. Farrugia, *J. Appl. Crystallogr.* **2012**, *45*, 849–854.

Received: April 29, 2015
Published Online: August 12, 2015

  